International Journal of Quantum Information
Vol. 12, Nos. 7 & 8 (2014) 1560015 (11 pages)

DOI: 10.1142/S0219749915600151





# Experimental hybrid entanglement between quantum and classical states of light

Luca S. Costanzo*, Alessandro Zavatta*, Samuele Grandi† and Marco Bellini*,‡

*Istituto Nazionale di Ottica (INO-CNR) and LENS,
50019 Sesto Fiorentino, Florence, Italy

†Centre for Cold Matter, Blackett Laboratory,
Imperial College London, London SW7 2AZ, UK
‡bellini@ino.it

Hyunseok Jeong, Minsu Kang and Seung-Woo Lee

Center for Macroscopic Quantum Control, Department of Physics and Astronomy,
Seoul National University, Seoul 151-742, South Korea

Timothy C. Ralph

Centre for Quantum Computation and Communication Technology,
School of Mathematics and Physics, University of Queensland, Qld 4072, Australia

Received 29 October 2014
Revised 9 November 2014
Accepted 13 November 2014
Published 17 December 2014

The realization of hybrid entanglement between a microscopic (quantum) and a macroscopic (classical) system, in analogy to the situation of the famous Schrödinger's cat paradox, is an important milestone, both from the fundamental perspective and for possible applications in the processing of quantum information. The most straightforward optical implementation of this condition is that of the entanglement between a single-photon and a coherent state. In this work, we describe the first step towards the generation of this type of hybrid entanglement from the experimental perspective.

*Keywords*: Hybrid entanglement; quantum optics; quantum state engineering.

## 1. Introduction

One of the fundamental and still open questions of quantum mechanics is related to the border between quantum and classical domains. It is well represented in the so-called Schrödinger's cat paradox,[1] where the states of a microscopic quantum system (an atom) and a macroscopic classical one (a cat) were assumed to be entangled.

‡Corresponding author.

In the optical domain, microscopic-macroscopic entanglement has recently been the subject of intense experimental research.[2–4] A possible optical implementation of the Schrödinger's cat entangled state can be realized considering the hybrid entanglement of the state of a single photon with that of a coherent state. Indeed, coherent states can be treated semiclassically (i.e. classical light with stochastic fluctuations) in many situations, and are therefore considered as a good picture of a macroscopic state of light. On the other hand, a single-photon constitutes the minimum, quantized amount of energy available in a given mode of light, so it represents the best example of a microscopic optical quantum system.

The ability to generate entanglement between these two kinds of systems would represent the optical analog of the Schrödinger's cat situation and could help to shed light on the quantum-to-classical transition mechanism.

Besides its fundamental implications, this new kind of hybrid entanglement can mark the start of a radically new line of quantum optical technologies that fully exploit the complementary wave and particle nature of light. The hybrid strategy combines two usually separated approaches, i.e. the discrete- and the continuous-variable (DV and CV) methods, into an integrated platform for quantum information processing, including communication, computing and metrology. In fact, optical quantum information processing schemes solely based upon either discrete or continuous degrees of freedom suffer from fundamental as well as practical limitations. DV schemes can achieve fidelities close to unity, but usually at the expense of probabilistic implementations which make them hard to scale. On the other hand, CV methods can benefit from unconditional (deterministic) operations, high detection efficiencies, unambiguous state discrimination and more practical interfacing with conventional information technology. However, they suffer from a strong sensitivity to losses and intrinsically limited fidelities. Moreover, the usual, so-called, Gaussian resources (states and operations) of the CV toolbox are not sufficient to execute important tasks like entanglement distillation, quantum error correction, nor universal quantum computing.

A hybrid scheme exploiting, at the same time, both DV and CV states, encodings, gates, measurements, and techniques, would allow one to circumvent most of those limitations and to develop unprecedented capabilities.[5,6] Furthermore, the generation of high-fidelity hybrid entangled states may allow the construction of interfaces between parts of a future heterogeneous quantum network where information can be transferred, manipulated, and stored, using different encodings according to the different physical platforms involved.

## 2. The Hybrid Entangled State

The hybrid entangled state considered in this work is

$$|\psi(\alpha_f)\rangle = \frac{1}{\sqrt{2}}(|0\rangle|\alpha_f\rangle + |1\rangle|-\alpha_f\rangle), \tag{1}$$

where $|0\rangle$ is the vacuum state, $|1\rangle$ the single-photon state, and $|\pm\alpha_f\rangle$ coherent states with amplitudes $\pm\alpha_f$.

As stated above, this state can be considered as the optical implementation of the Schrödinger's Gedanken experiment, as it manifests entanglement between quantum (single-photon) and classical (coherent) states of light. The degree of entanglement depends on the amplitude $\alpha_f$ of the coherent state component: The state becomes factorizable for $\alpha_f \to 0$; on the other hand, it becomes more entangled the more macroscopic the classical part is, i.e. in the limit of $\alpha_f \gg 1$, when the two coherent states $|\pm\alpha_f\rangle$ minimize their overlap.

So far, the main proposals for the generation of this kind of hybrid entangled states[7–9] were based on cross-Kerr interaction of single photons and coherent states in a crystal; however, it is well known that this type of nonlinearity is extremely difficult to achieve in practice.

In this work we describe an accessible scheme[10] for the generation of hybrid entanglement of the form of Eq. (1). The main advantage of our approach and of similar ones[11] recently demonstrated, is that it is not based on cross-Kerr interaction, but simply relies upon the realization of a superposition of photon creation operations on two distinct modes.

One may first observe that a single-photon-added coherent state (SPACS),[12,13] $|\alpha,1\rangle$, the result of the application of the photon creation operator onto a coherent state with amplitude $\alpha$, can well approximate another coherent state of larger amplitude $g\alpha$, with the gain factor $g \geq 1$:

$$\frac{\hat{a}^\dagger}{\sqrt{1+|\alpha|^2}}|\alpha\rangle = |\alpha,1\rangle \approx |g\alpha\rangle \tag{2}$$

with the normalization factor $1/\sqrt{1+|\alpha|^2}$. The fidelity between the SPACS and a larger coherent state can be easily calculated as

$$\mathcal{F} = \left| \langle g\alpha| \frac{\hat{a}^\dagger}{\sqrt{1+|\alpha|^2}}|\alpha\rangle \right|^2 = \frac{g^2|\alpha|^2 e^{-|\alpha|^2(g-1)^2}}{1+|\alpha|^2} \tag{3}$$

and it is maximized when $g$ is equal to its optimal value

$$g_{\text{opt}} = \frac{1}{2} + \sqrt{\frac{1}{4} + \frac{1}{|\alpha|^2}}. \tag{4}$$

For large coherent state amplitudes, i.e. in the limit of $\alpha \gg 1$, the gain decreases ($g_{\text{opt}} \to 1$), but the fidelity of the SPACS to a larger coherent state $|g_{\text{opt}}\alpha\rangle$ reaches the maximum value, $\mathcal{F} \to 1$. For small coherent state amplitudes, the gain becomes larger, but the corresponding fidelity of the resulting SPACS to a coherent state decreases. A value $\mathcal{F} \approx 0.95$ can be obtained with an initial coherent state $\alpha \approx 1.5$.

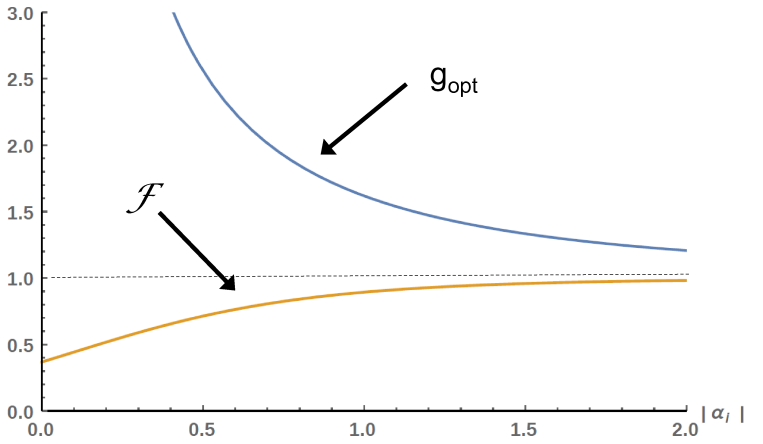


Fig. 1. Optimized gain and fidelity between a SPACS and a larger coherent state. The optimized gain $g_{\text{opt}}$ (Eq. (4)) is defined as the gain $g$ that maximizes the fidelity between the SPACS $\hat{a}^\dagger|\alpha\rangle$ and the coherent state $|g\alpha\rangle$ as a function of $\alpha$. The plotted fidelity is the one calculated for such an optimal gain.

The next step, is the implementation of the superposition

$$re^{i\phi}\hat{a}_1^\dagger + t\hat{a}_2^\dagger, \tag{5}$$

where $\phi$ is the relative phase between the coefficients $r$, $t$, taken as real.

This kind of operation can be implemented by using two single-photon-addition devices on modes 1 and 2. The single-photon addition operation can be experimentally realized in the signal mode of a low-gain parametric down-converter upon detection of an idler photon.[13,14] If we mix the heralding idler photons of two down-converters onto a beam-splitter (BS) of transmittivity $t$ and reflectivity $r = \sqrt{1-t^2}$ with a relative phase $\phi$, a click in a single-photon detector at one of the outputs erases the information as to which of $\hat{a}_1^\dagger$ or $\hat{a}_2^\dagger$ occurred, while making sure that one of these two events certainly happened.[15]

In our work, the operation (5) is applied to the initial state $|0\rangle_1|\alpha_i\rangle_2$[a]

$$\begin{aligned}|\psi\rangle_{12} &= \sqrt{\frac{1}{1+t^2|\alpha_i|^2}}(r\hat{a}_1^\dagger + t\hat{a}_2^\dagger)|0\rangle_1|\alpha_i\rangle_2 \\ &= \sqrt{\frac{1}{1+t^2|\alpha_i|^2}}(r|1\rangle_1|\alpha_i\rangle_2 + t\hat{a}_2^\dagger|0\rangle_1|\alpha_i\rangle_2).\end{aligned} \tag{6}$$

The photon addition can thus either take place in the first mode, creating a single photon $|1\rangle_1$ and leaving unchanged the initial coherent state $|\alpha_i\rangle_2$ or in the second one, leaving the vacuum $|0\rangle_1$ and producing a SPACS $\hat{a}_2^\dagger|\alpha_i\rangle_2$ in the second mode.

[a] The signal mode of the first down-converter is not seeded, whereas a coherent state is injected in the signal mode of the second.

The factor $\sqrt{1/(1+t^2|\alpha_i|^2)}$ is the global normalization factor and the phase $\phi$ has been set to 0 for simplicity in this case.

It is important to note that the state $\hat{a}_2^\dagger|\alpha_i\rangle_2$ is not normalized (see Eq. (2)); therefore, a balanced superposition in Eq. (6) cannot be simply obtained by using a 50% beam-splitter, because the coefficients of the superposition itself do not depend on the reflectivity only. The intuitive reason is that the photon addition in the second down-converter is a stimulated process and is therefore more likely than the spontaneous one in the first. The ratio between the two depends on the mean photon number in the injected signal mode so, in the case of coherent state seeding, it is $1+|\alpha|^2$. In order to balance the two terms of the entangled state, this difference should be compensated by adjusting the BS transmittivity $t$ as:

$$t = (\alpha_i^2 + 2)^{-1/2}, \tag{7}$$

as obtained by imposing

$$\begin{cases} \dfrac{|r|^2}{|t|^2} = 1 + |\alpha_i|^2 \\ |r|^2 + |t|^2 = 1. \end{cases} \tag{8}$$

The BS setting, that is the value $t$ that makes the superposition balanced, therefore depends on $\alpha$.

Once the probabilities are balanced, the resulting state becomes

$$|\psi_O\rangle_{12} = \frac{1}{\sqrt{2}}\left(|1\rangle_1|\alpha_i\rangle_2 + \frac{\hat{a}_2^\dagger}{\sqrt{1+|\alpha_i|^2}}|0\rangle_1|\alpha_i\rangle_2\right) \approx \frac{1}{\sqrt{2}}(|1\rangle_1|\alpha_i\rangle_2 + |0\rangle_1|g\alpha_i\rangle_2). \tag{9}$$

The state of Eq. (9) already presents the desired kind of entanglement between a single photon and a coherent state but it is not yet in the symmetric form of Eq. (1), which is usually considered as the basis for quantum information processing.[5] In order to achieve the desired form, one can we apply a displacement operator on mode 2 that translates back both coherent states $|\alpha_i\rangle_2$ and $g|\alpha_i\rangle_2$ towards the origin of phase-space by an amount corresponding to their center of gravity $1/2(\alpha_i + g\alpha_i)$ such that

$$|\psi_S\rangle_{12} = \hat{D}_2\Big(-\frac{\alpha_i + g\alpha_i}{2}\Big)|\psi_O\rangle_{12} \approx |\psi(\alpha_f)\rangle_{12} = \frac{1}{\sqrt{2}}(|0\rangle_1|\alpha_f\rangle_2 + |1\rangle_1|-\alpha_f\rangle_2) \tag{10}$$

with

$$\alpha_f = (g\alpha_i - \alpha_i)/2. \tag{11}$$

## 3. Experimental State Generation

The experimental generation of small-scale hybrid entangled states is implemented by using the idea depicted above of a coherent superposition of two single-photon-addition operations onto two distinct modes containing the vacuum and a coherent

state. Our approach makes use of two different traveling wavepacket temporal modes, instead of spatial ones, along the line of Franson's-type[16] experiments and of time-bin encoding of quantum information.[17] The particular scheme adopted in our experiment was first developed and used for the remote generation of temporally delocalized single-photon states[18] and has several practical advantages compares to its spatial-mode version. By operating in the time domain on the same spatial mode, a single parametric down-converter is required for implementing photon addition, and a single homodyne detector suffices for the analysis of the two modes.

The basic light source for the experiment is a 1.5 ps mode-locked Ti:sapphire laser centered at 785 nm, and with a repetition rate of 80 MHz. The pump radiation for the parametric down-conversion is obtained by frequency-doubling the laser light in a LBO crystal (see Fig. 2). We produced the temporal version of the superposition of single-photon addition operators (Eq. (5)), by passing the idler photons emitted by a type-I parametric down-conversion BBO crystal through an unbalanced Mach–Zehnder interferometer based on single-mode fibers. Idler light is coupled into the interferometer after being spectrally filtered by means of a couple of etalon filters tuned to the laser wavelength. This spectral filter is essential to produce a pure state instead of a mixture in the signal mode.

When an idler photon is detected at one of the outputs of the interferometer it is not possible to distinguish, not even in principle, if it passed through the short or the long arm; as a consequence, the superposition $r\hat{a}^{\dagger}_{t_1} + \sqrt{1-r^2}\hat{a}^{\dagger}_{t_2}$ is heralded onto the two temporal modes $t_1$ and $t_2$ in the signal mode. The delay $(t_2 - t_1)$, defined as

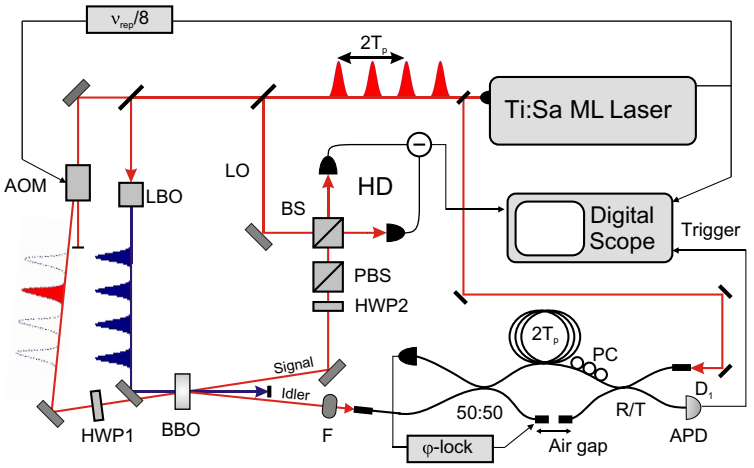


Fig. 2. Experimental scheme for the generation of the hybrid symmetric entangled state. To avoid any contamination between different temporal modes during homodyne detection, we encode the analyzed temporal modes in non-consecutive pulses, by choosing a delay of twice the inverse of the repetition rate $\nu_{\rm rep} = 1/T_p$. The AOM is triggered by a 10 MHz trigger signal synchronized with the laser pulse train. The phase of the Mach–Zehnder interferometer is locked by monitoring the interference signal in a counter-propagating laser pulse train.

the difference between the two optical paths in the Mach–Zehnder interferometer, was made equal to twice the temporal difference $T_p$ between successive pulses in the laser train ($2T_p \approx 24\,\text{ns}$). In principle, one could simply choose $T_p$ as the time separation between the two analyzed modes, but we decided to use $2T_p$ instead, to improve the discrimination of the modes during the homodyne detection.

As previously discussed, in order to obtain the state of Eq. (6) we need to seed the signal mode of the parametric crystal with the state $|0\rangle_{t_1}|\alpha_i\rangle_{t_2}$, given by vacuum in the first temporal mode and a coherent state of amplitude $\alpha_i$ in the second. For this purpose, an acousto-optic modulator (AOM) has been inserted in the path of an attenuated portion of the laser pulse train to work as a pulse-picker. In principle, one could operate the AOM at a rate given by the inverse of the delay imposed by the interferometer, i.e. about 40 MHz. However, bandwidth limitations in the AOM driver and trigger electronics forced us to use a lower rate of about 10 MHz. The AOM thus transmits one in every eight pulses of the train and reduces the acquisition rate of the experiment at least by a factor of 8. Considering the losses in the interferometer and the fact that we only use one of its outputs, the overall acquisition rate of this experiment may drop by almost two orders of magnitude if compared to a typical single-mode photon addition case.

By adjusting the relative transmission and delay between the long and short arm of the interferometer while injecting the two-mode signal state, it is possible to explore the whole range of coefficients and relative phases of the superposition ($t, \phi$ in Eq. (5)). For this purpose, we regulated a variable-ratio fiber coupler and used piezoelectric transducers for a fine adjustment of the free-space propagation parts in the Mach–Zehnder interferometer.

As already mentioned above, to generate the balanced state of Eq. (9) two conditions must be fulfilled: the first is defined by Eq. (8), the second fixes the relative phase $\phi = 0$. To achieve this, we adjusted the splitting ratio of the fiber coupler in order to equalize the idler count rates due to each of the two interferometer arms, rather than simply fixing it at 50% reflectivity. Indeed, photon count rates in the short and long paths are proportional to the probabilities of stimulated and spontaneous parametric emission and, in the balanced case, the two terms should be equalized by properly adjusting the coupler reflectivity.

The phase $\phi$ of the superposition is controlled by the relative fine delay between the two optical paths in the interferometer. We monitor such a relative phase by injecting a part of the laser emission through the unused exit port of the interferometer and detecting the interference fringes at the unused input. By actively locking the piezoelectric transducers to a given value of the interference signal, a stable superposition phase is achieved. In particular, we set it to 0 by locking the interferometer to a fringe maximum.

Finally, we performed a coherent displacement on the second temporal mode of the entangled state and produce the symmetric state of Eq. (10). A coherent phase-space displacement on a single-mode quantum field is usually implemented experimentally

by mixing it with an intense coherent state on a low-reflectivity beam-splitter. Here we do it only on a well-defined temporal mode of a two-temporal-mode entangled state; therefore, an accurate and phase-stable spatial and temporal matching between the signal and the displacement coherent state has to be guaranteed.

We exploited the polarization degree of freedom at this purpose: By using a slightly-rotated half-wave-plate (HWP1) before the BBO crystal, we introduced a horizontal component to the vertically-polarized 10 MHz pulse train coming from the AOM. While the vertical component of the injected coherent states kept serving as the seed for the down-conversion, their synchronized horizontal component passed unaffected through the BBO crystal. The two components were then mixed again with the appropriate ratio by another half-wave-plate (HWP2) after the BBO and before a polarizing beam-splitter (PBS) selected the vertical component for subsequent homodyne analysis.



## 4. State Detection and Analysis

As already observed, the heralded approach followed in this experiment implies that the generation of the state is conditioned on some events. By triggering the detection on the periodic signal at 10 MHz used to drive the AOM, we guarantee the presence of the injected coherent state in the signal mode at time $t_2$ ($|0\rangle_{t_1}|\alpha_i\rangle_{t_2}$). The second conditional event is the detection of an idler photon after the interferometer, necessary to cause the collapse of the wave function onto the desired state (see (6)). In addition, to reduce the dark counts in the idler channel, we synchronized the detection with the laser pulse train at 80 MHz.

We performed independent quadrature measurements on both the temporal modes of interest by time-domain balanced homodyne detection at the two corresponding times. The local oscillator for the homodyne detection scheme is a 80 MHz pulse train coming from the same source laser. Each measurement is composed of a pair of quadrature values $x_{t_1}(\theta_{t_1}), x_{t_2}(\theta_{t_2})$ with the phases $\theta_{t_1}$, $\theta_{t_2}$ defined by the local oscillator phases for pulses at times $t_1$ and $t_2$. In principle, one should acquire quadrature measurements while performing a full scan of the two phases $\theta_{t_1}$ and $\theta_{t_2}$ independently. However, since it is technically quite demanding to carefully adjust the relative phase between successive pulses in the local oscillator train, we followed an alternative but, from the mathematical point of view, perfectly equivalent, approach. We kept the relative LO phases fixed and scanned the superposition phase of the entangled state instead.

In fact, let us consider the application of the creation operator superposition of Eq. (5) onto a two-mode state containing a Fock state in the first mode:

$$|\chi\rangle_{12} = (re^{i\phi}\hat{a}_1^\dagger + t\hat{a}_2^\dagger)|n\rangle_1|\psi\rangle_2 = r\sqrt{n+1}e^{i\phi}|n+1\rangle_1|\psi\rangle_2 + t|n\rangle_1|\psi'\rangle_2 \tag{12}$$

with $|\psi'\rangle_2 = \hat{a}_2^\dagger|\psi\rangle_2$. We stress that we are considering a general state subjected to the only condition of having a Fock state on one of the two modes. Let us now

calculate the two-mode quadrature probability distribution

$$\begin{aligned} P[x_1(\theta_1), x_2(\theta_2)] &= |\langle x_1(\theta_1)|\langle x_2(\theta_2)|\chi\rangle_{12}|^2 \\ &= |re^{i\phi}\sqrt{n+1}e^{i(n+1)\theta_1}\langle x_1|n+1\rangle\langle x_2(\theta_2)|\psi\rangle \\ &\quad + te^{in\theta_1}\langle x_1|n\rangle\langle x_2(\theta_2)|\psi'\rangle|^2 \\ &= r^2(n+1)P_{n+1}[x_1]P_{\psi}[x_2(\theta_2)] + t^2P_n[x_1]P_{\psi'}[x_2(\theta_2)] \\ &\quad + e^{i(\phi+\theta_1)}r\sqrt{n+1}\,t\langle x_1|n+1\rangle\langle x_1|n\rangle\langle x_2(\theta_2)|\psi\rangle\langle x_2(\theta_2)|\psi'\rangle + c.c. \\ &= P[x_1(\theta_1+\phi), x_2(\theta_2)], \end{aligned} \tag{13}$$

where we have used the fact that $\langle x(\theta)|n\rangle = e^{i\theta}\langle x|n\rangle$ and $P_n[x(\theta)] = |\langle x|n\rangle|^2$ is the phase-independent quadrature distribution for the Fock states. The full two-mode quadrature probability distribution is only seen to depend on the LO phase $\theta_2$ and on the sum of the LO phase in the first mode $\theta_1$ and of the superposition phase $\phi$, whose roles are thus interchangeable. Therefore, for the class of states investigated here, it is possible, and perfectly equivalent, to perform quantum tomography by using a common local oscillator phase for the two modes ($\theta = \theta_{t_1} = \theta_{t_2}$) and varying the state superposition phase $\phi$, instead of keeping the state fixed and scanning the two LO phases during the homodyne acquisition.

About $6 \times 10^5$ quadrature pairs are acquired to perform the full tomography of each state using a two-mode extended maximum-likelihood-based algorithm.[19,20] The dimensions of the reconstructed density matrices in the Fock basis are adjusted to the size of the investigated states. Therefore, three terms in the Fock expansion are normally used for the first mode (ideally containing just vacuum and single-photon components), whereas up to 25 are necessary for the second mode, containing the coherent and the photon-added coherent states. When dealing with the symmetric hybrid entangled state after phase-space displacement, the effective amplitude of the coherent states $|\pm\alpha_f\rangle$ in the symmetric superposition is relatively small and also the number of reconstructed matrix elements for the second mode is thus reduced accordingly.

## 5. Results and Conclusion

Figure 3 shows the reconstructed density matrix for the experimental hybrid state $|\psi_O\rangle_{12}$ in the two-mode Fock base. It shows a blocks structure, where each block is related to a given pair of Fock states in the first mode. As expected, the yellow block, corresponding to vacuum in the first mode, represents a photon-added coherent state, while the blue block, corresponding to a single photon in the first mode, represents an unperturbed coherent state. The off-diagonal blocks show the high coherent nature of the entangled state. The almost negligible red terms indicate the real single-photon nature of the state in the first mode.

In conclusion, we have described a new experimental scheme for the generation of hybrid quantum-classical entangled states based on the superposition of non-Gaussian quantum operators on multiple modes. With respect to other approaches, our

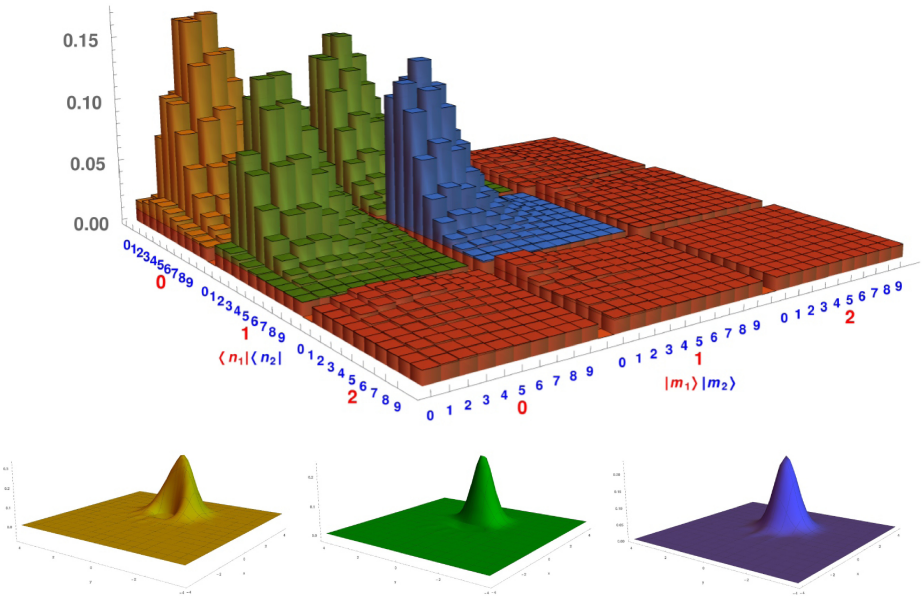


Fig. 3. (Color online) Reconstructed density matrix of the generated hybrid state. The density matrix $\hat{\rho} = |\psi_O\rangle_{12}\langle\psi_O|_{12}$ of the hybrid state of Eq. (9) with $\alpha_i \approx 1.4$ has been reconstructed in the two-mode Fock base $|m_1\rangle|m_2\rangle$, respectively limited to 2- and 9-photon components; we corrected for a detection efficiency of 61%. For the sake of clarity, we used different colors for each block: The yellow part is the SPACS term $|\alpha, 1\rangle\langle\alpha, 1|$; the blue is related to the coherent state $|\alpha\rangle\langle\alpha|$; the two green blocks are the coherence term $|\alpha, 1\rangle\langle\alpha|$, and its hermitian transposed; the red ones are the blocks containing two-photon terms in the first mode. With the same colors we show the experimental Wigner functions corresponding to each block.

proposal uses only currently available resources and does not require unrealistically strong cross-Kerr nonlinearities.

This result may allow the implementation of deterministic quantum logic gates based on linear optics and specifically designed for hybrid qubits. Another possible application could be the implementation of hybrid quantum teleportation protocols between wave-like (coherent state) and particle like (single-photon) states,[21] in order to build a interface for future heterogeneous networks using both CV and DV states.

## Acknowledgments

This work was partially supported by European Union under the CHIST-ERA project QSCALE (Quantum Technologies for Extending the Range of Quantum Communications) and from the Italian Ministry of Education, University and Research under the FIRB contract No. RBFR10M3SB.

## References

1. E. Schrödinger, *Naturwissenschaften* **23** (1935) 823.
2. F. De Martini, F. Sciarrino and C. Vitelli, *Phys. Rev. Lett.* **100** (2008) 253601.

3. A. I. Lvovsky, R. Ghobadi, A. Chandra, A. S. Prasad and C. Simon, *Nat. Phys.* **9** (2013) 541.
4. N. Bruno, A. Martin, P. Sekatski, N. Sangouard, R. T. Thew and N. Gisin, *Nat. Phys.* **9** (2013) 545.
5. S.-W. Lee and H. Jeong, *Phys. Rev. A* **87** (2013) 022326.
6. H. Kwon and H. Jeong, *Phys. Rev. A* **88** (2013) 052127.
7. C. Gerry, *Phys. Rev. A* **59** (1999) 4095.
8. K. Nemoto and W. J. Munro, *Phys. Rev. Lett.* **93** (2004) 250502.
9. H. Jeong, *Phys. Rev. A* **72** (2005) 034305.
10. H. Jeong, A. Zavatta, M. Kang, S. Lee, L. S. Costanzo, S. Grandi, T. C. Ralph and M. Bellini, *Nat. Photon.* **8** (2014) 564.
11. O. Morin, K. Huang, J. Liu, H. Le Jeannic, C. Fabre and J. Laurat, *Nat. Photon.* **8** (2014) 570.
12. G. S. Agarwal and K. Tara, *Phys. Rev. A* **43** (1991) 492.
13. A. Zavatta, S. Viciani and M. Bellini, *Science* **306** (2004) 660.
14. V. Parigi, A. Zavatta, M. S. Kim and M. Bellini, *Science* **317** (2007) 1890.
15. A. Zavatta, V. Parigi, M. S. Kim, H. Jeong and M. Bellini, *Phys. Rev. Lett.* **103** (2009) 140406.
16. J. D. Franson, *Phys. Rev. Lett.* **62** (1989) 2205.
17. J. Brendel, N. Gisin, W. Tittel and H. Zbinden, *Phys. Rev. Lett.* **82** (1999) 2594.
18. A. Zavatta, M. D'Angelo, V. Parigi and M. Bellini, *Phys. Rev. Lett.* **96** (2006) 020502.
19. A. I. Lvovsky, *J. Opt. B* **6** (2004) S556.
20. Z. Hradil, J. Řeháček, E. Knill and A. I. Lvovsky, *Phys. Rev. A* **75** (2007) 042108.
21. K. Park, S.-W. Lee and H. Jeong, *Phys. Rev. A* **86** (2012) 062301.